Article | Received 10 November 2025; Revised 15 December 2025; Accepted 4 January 2026; Published 26 January 2026
https://doi.org/10.55092/sc20260002

Comparison and selection of support schemes for deep buried soft broken section of Xinjin expressway spiral tunnel—a case study of Hankou tunnel

Dechun Lu[1], Xiaoyu Liu[1], Haining Xu[2], Caixia Guo[1,*] and Xiuli Du[1]

[1] College of Architecture and Civil Engineering, Beijing University of Technology, Beijing, China
[2] China Construction Road and Bridge Group Fourth Engineering Co., Ltd., Zhengzhou, China

* Correspondence author; E-mail: guocaixia@bjut.edu.cn.

Highlights:

- Four finite element models with refined simulation of the entire construction process are established and highly consistent with field monitoring data.
- Displacement evolution patterns throughout different construction stages is thoroughly analyzed.
- The use of advanced small pipes serves as an auxiliary construction method in soft and fractured sections, providing pre-reinforcement to the surrounding rock.
- A combined scheme of primary support, secondary lining and systematic rock bolts proves effective in deep-buried mountain tunnels.

Abstract: Based on the spiral tunnel group of Xinjin expressway, this paper takes the typical deep buried soft broken section of Hankou tunnel as the research object. On the basis of the composite lining structure with primary support and secondary lining, considering four working conditions: the presence or absence of systematic rock bolts and advanced small pipes. Utilizing the ABAQUS numerical simulation platform, refined numerical simulations of the entire construction process are conducted and compared with field-measured engineering data. The results indicate: (1) Under all four working conditions, the vault settlement and horizontal convergence exhibit a pattern of slow growth, followed by rapid growth, and eventual stabilization during tunnel excavation. When excavating the core soil of the upper bench after installing the primary support, the rate and magnitude of change in vault settlement and horizontal convergence are significant. However, after installing the secondary lining, the rates of change for both remain relatively stable; (2) The application of systematic rock bolts effectively controls vault settlement, horizontal convergence, and plastic zones in the surrounding rock. The use of advanced small pipes demonstrates good control over vault settlement and stress in the surrounding rock; (3) In terms of controlling vault stress in the surrounding rock, advanced small pipes outperform systematic rock bolts, whereas systematic rock bolts are more effective than advanced small pipes in controlling horizontal convergence, maximum tensile stress, and plastic zones; (4) Considering both numerical simulation results and the construction cost analysis, the combined use of primary support, secondary lining, and systematic rock bolts is sufficient to effectively control the stress and deformation of the surrounding

rock. Advanced small pipes can serve as an auxiliary construction method in soft and fractured sections, providing pre-reinforcement to the surrounding rock.

Keywords: expressway spiral tunnel; deep buried soft and weak surrounding rock; comparison and selection of multiple support schemes; refined simulation of the entire construction process

1. Introduction

In recent years, with the economic growth and the implementation of the National Strength in Transportation strategy, Chinese transportation infrastructure has experienced rapid development, gradually expanding from urban areas to mountainous regions. China boasts a vast territory with complex and diverse topographic and geological conditions, where mountainous areas account for over 69.1% of the total land area. In such complex terrain, mountain tunnels are playing an increasingly critical role in modern transportation systems, leading to the continuous emergence of numerous long, deep-buried mountain tunnel projects. However, owing to the intricate and variable geological conditions along the routes, the construction of deep-buried mountain tunnels is likely to encounter engineering challenges such as cracking and misalignment of concrete structures, fracture of steel arches, collapses, and water inrushes [1–7]. These issues necessitate higher demands for the design and construction of tunnel support systems.

Currently, the construction design philosophy for mountain tunnels in China is predominantly based on the New Austrian Tunneling Method (NATM). Support is typically provided by a composite lining system, which integrates an initial support comprised of shotcrete, steel arches, and rock bolts with a secondary lining. In sections with adverse geological conditions, auxiliary measures such as advanced rock bolts, advanced small pipes, and pipe canopies are generally employed for pre-support and pre-reinforcement. These measures can ensure the stability of the surrounding rock and guarantee safety during tunnel construction.

Systematic rock bolts, as a crucial component of shotcrete and rock bolt support, have been widely adopted in tunnel construction. Several studies have focused on the support effectiveness of systematic rock bolts. One study employed a combined approach of field monitoring and numerical simulation to analyze the stress characteristics of rock bolts in a large-span shallow-buried tunnel. Significant differences were found in the axial forces of rock bolts at different locations, leading to the proposal of a non-uniform support design concept [8]. Zhou conducted research on the load-bearing mechanism of composite linings in deep-buried tunnels through theoretical analysis, numerical simulation, and model tests. The results indicated that poorer surrounding rock conditions would lead to a more pronounced increasing trend in axial force, and that the effect of rock bolts was particularly significant at the vault and arch springing [9]. Bobet *et al.* derived analytical solutions for the convergence deformation of surrounding rock and the support loads under the reinforcement of DMFC rock bolts *versus* CMC or CFC rock bolts. They conducted a comparative analysis of the support effects of different bolt types and validated their findings through numerical simulations [10]. Chen *et al.* performed geomechanical model tests which demonstrated that the inclusion of rock bolts in weak interlayers with dip angles of 30 ° and 60 ° altered the failure mode, resulting in an overall splitting failure and achieving the optimal support effect [11]. Model tests were used in another research in order to study the bearing capacity of a two-lane highway tunnel in Grade Ⅳ surrounding rock under different support systems. The results showed that

the ultimate bearing capacities under three support scenarios were significantly higher than that of an unsupported tunnel. The combination of systematic rock bolts and shotcrete provided the best support effect, followed by shotcrete alone, and then systematic rock bolts alone [12].

However, some scholars believe that the reinforcement effect of the system rock bolts is limited. Tan *et al.* studied the support effect of the system rock bolts under the condition of large section and deep buried old loess stratum. Comparative test results indicated that while the sidewall rock bolts sustained considerable tension and played a certain supportive role, the systematic rock bolts in the arch section exhibited a negligible support effect [13]. In another research, scholars carried out a large number of field tests on the support effect of the system rock bolts. It was similarly revealed that most systematic rock bolts in the tunnel vault were in a state of compression, resulting in poor support performance and indicating room for optimization [14]. Sun *et al.* conducted a comparative test with and without the system bolt, and found that the support effect of the system bolt was not obvious for the deep buried tunnel with moderately weathered mudstone [15].

On the other hand, the advanced small pipe, as a type of pre-support measure, offers advantages such as straightforward construction, high adaptability, and favorable waterproofing performance. Numerous studies have been conducted to explore the support effectiveness of advanced small pipes. Jin *et al.* simulated and analyzed the plastic zone, displacement, and stress field of the surrounding rock with and without advanced small pipe support. They proposed that advanced small pipes represented an effective and advanced support method for tunneling in weak and fractured rock masses [16]. Qin *et al.* utilized the finite difference software FLAC3D to simulate the grouting support effect of advanced small pipes in large-section tunnels with weak surrounding rock. The results demonstrated that advanced small pipes created a canopy effect, effectively altering the mechanical properties of the surrounding rock and thereby enhancing its stability [17]. Liu *et al.* elucidated the mechanism of advanced small pipe support through numerical simulations combined with field tests. Their research found that advanced small pipes expanded the range of the bearing arch, reduced the vertical load acting on the tunnel face, and simultaneously improved the early-stage utilization rate of the lining structure [18]. Lin *et al.* employed theoretical analysis to investigate the stability of the tunnel face under the influence of advanced small pipes. Numerical simulations were conducted in order to discuss the effects of various parameters on both the pipe roof deflection and face stability [19]. Wang *et al.* studied the deformation control in soft rock tunnels with small clear distances. Using a combination of numerical simulation and field monitoring, they found that advanced small pipes could significantly reduce deformation values, with a maximum reduction of approximately 20% [20]. Zhang *et al.* conducted numerical simulation and field monitoring research addressing the pre-support challenges for a shallow-buried water-rich fault fracture zone tunnel passing beneath a provincial highway. They compared the support effectiveness of three pre-support schemes: advanced small pipes alone, a pipe roof alone, and a combination of advanced small pipes and a pipe roof. Their study ultimately recommended the adoption of the combined support scheme utilizing both advanced small pipes and a pipe roof [21].

In summary, the working mechanisms of systematic rock bolts have not been fully elucidated, and the support effectiveness in tunnels remains contentious at present. Meanwhile, the advanced small pipe, as a form of pre-support, has been the subject of limited research regarding its combined support effect when used alongside systematic rock bolts. Therefore, this paper presents a study based on the Hankou tunnel project—a typical deep-buried section within weak and fractured strata that is part of the Xinjin

expressway spiral tunnel group. Utilizing numerical simulations combined with field monitoring, and building upon a composite lining structure of initial and secondary support, the research investigates four working conditions considering the presence and absence of both systematic rock bolts and advanced small pipes. It provides a detailed analysis of the support effects of different schemes in deep-buried tunnels under weak and fractured rock conditions, aiming to offer engineering references for supporting deep-buried mountain tunnels under similar geological conditions.

2. Engineering background

2.1. Project overview

The Xinjin expressway is a high-speed corridor along the Taihang Mountains, connecting Henan and Shanxi provinces. It starts at Kuaicunying Village in Xinxiang City, Henan Province, and ends at Yingpan Village in Lingchuan County, Shanxi Province, with a total length of 69.75 km. It is a crucial component of the expressway network in Northern Henan and also serves as a vital shortcut linking Northwestern Henan with Southeastern Shanxi. The bridge-tunnel section of the Xinjin expressway spiral tunnel group spans 28 km, entirely situated within the deep mountainous area of the Southern Taihang Mountains at elevations between 500 m and 1,280 m above sea level. This section comprises nine tunnels, overcoming a total vertical drop of 780 m. The entire spiral tunnel group ascends through the Jiaoding Mountains of the Southern Taihang range in a winding, spiral configuration. A schematic diagram of the project is shown in Figure 1. Constructed on near-vertical cliff faces, the spiral tunnel group presented immense construction challenges and required stringent control of surrounding rock deformation.

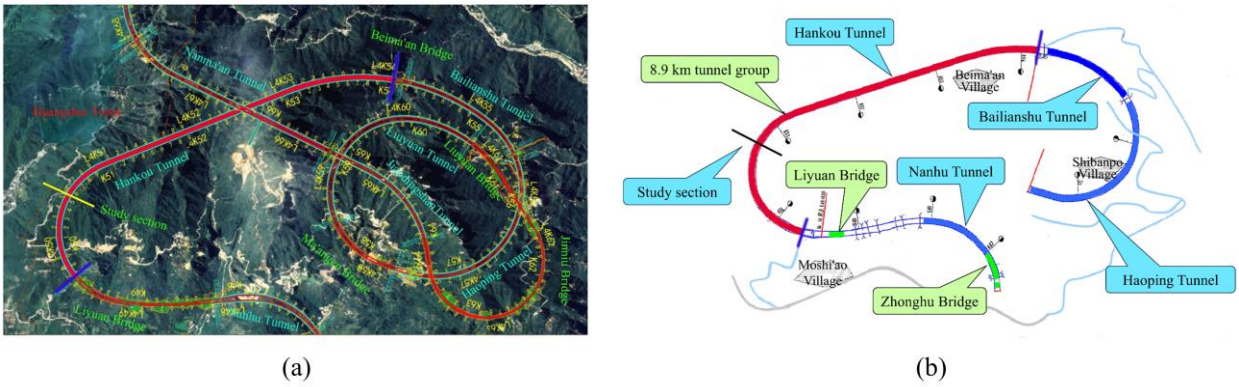

Figure 1. Schematic diagram of Xinjin spiral tunnel group project profile. **(a)** Satellite cloud image; **(b)** Schematic diagram.

The Hankou tunnel is located in the hinterland of the Taihang Mountains in Huixian City, Henan Province. It constitutes a section of the Xinjin expressway and is a key controlled project of the expressway. The tunnel has a total length of 4,459 meters, spanning an elevation between 784 meters and 893 meters with an elevation difference of 109 meters between its portal and exit, and a minimum curve radius of 700 meters. On May 15, 2024, the Hankou tunnel was officially certified on-site by Guinness World Records as the "World's Longest Highway Spiral Tunnel." The tunnel alignment traverses small-scale structural fracture zones characterized by intensely fractured rock mass and high-water content. The study section selected for this paper is a deep-buried segment within a weak and fractured zone, classified as Grade V surrounding rock. It is situated in the middle of the left line of the Hankou tunnel, at chainage

Lk50+530 to Lk50+560. This segment is a deep-buried section with an approximate depth of 180 meters. The lithology primarily consists of moderately weathered sandstone. Due to tectonic influence, the rock mass features well-developed joints and fissures, resulting in a relatively fragmented core. The surrounding rock exhibits poor stability, with frequent sidewall spalling and collapses. During construction, water inflow phenomena, ranging from dripping to steady flows, were observed. The construction employed the Core Soil Method with Annular Excavation for tunnel advance.

2.2. Field support measures and configured working conditions

For the Grade V surrounding rock section of the Hankou tunnel, the implemented support measures included advanced small pipes, initial support, systematic rock bolts, and a secondary lining. The specific design parameters were as follows:

(1) Pre-support: A single layer of advanced small pipes was installed, covering a 120 °arc at the tunnel crown. Each pipe had a length of 4.5 m, a diameter of 42 mm, a circumferential spacing of 40 cm, and a longitudinal spacing of 320 cm.

(2) Initial support:

(a) A 24 cm thick shotcrete, with a strength grade of C25.

(b) Steel ribs using I-18 steel sections, with a longitudinal spacing of 0.8 m.

(c) A single layer of A6 steel mesh with a grid spacing of 15 cm × 15 cm.

(3) Systematic rock bolts: C22 grouted rock bolts were used, with a length of 3.0 m. They were arranged in a staggered pattern with a circumferential spacing of 120 cm and a longitudinal spacing of 80 cm.

(4) Secondary lining: A 45 cm thick, cast-in-place, waterproof concrete with a strength grade of C30.

In order to validate the rationality of the field-implemented support measures and their parameters, and to compare the reinforcement effects of different support combinations with or without systematic rock bolts and advanced small pipes, the following four support schemes were established for comparison, as detailed in Table 1. Given that the addition of feet-lock bolts resulted in only a 1.86% reduction in crown settlement and a 1.32% reduction in horizontal convergence, they were not considered in the computational scenarios configured for this study.

Table 1. Working conditions under different support schemes.

Working condition	Support scheme combination
Working condition 1	Initial support + Secondary lining
Working condition 2	Initial support + Secondary lining + Systematic rock bolts
Working condition 3	Initial support + Secondary lining + Advanced small pipes
Working condition 4	Initial support + Secondary lining + Systematic rock bolts + Advanced small pipes

3. Modeling methodology

3.1. Establishment of the tunnel excavation numerical model

A finite element numerical model for tunnel excavation was established using the ABAQUS numerical simulation platform, as illustrated in Figure 2. The overall dimensions of the numerical model were

140 m × 30 m × 230 m (x × y × z), with the tunnel advancing along the y-axis direction. The tunnel featured a horseshoe-shaped cross-section with a width of 10.90 m and a height of 8.59 m. The burial depth at the tunnel crown was 174.55 m. The model's lateral width of 140 m was 12.84 times the tunnel excavation width, and the distance from the tunnel center to the bottom boundary was 50 m, which was 5.82 times the tunnel excavation height. These dimensions satisfied the requirements for encompassing the tunnel's influence zone and effectively minimized the impact of boundary effects on the calculation results [22,23]. The model's top surface was set as a free boundary without any constraints. The bottom boundary was defined as a fixed support, restraining both tangential and normal displacements. The lateral boundaries were assigned as roller supports, constraining only the normal displacement at each respective boundary.

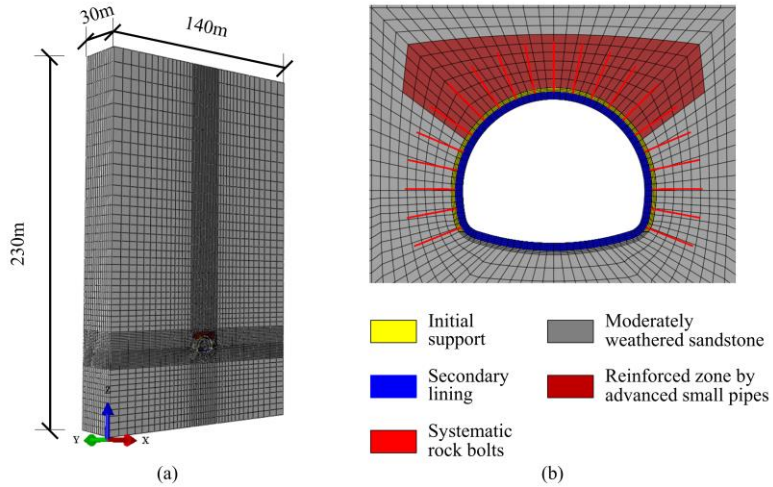

Figure 2. FEM model of the tunnel. **(a)** Overall view of the model; **(b)** Detailed view of the model.

In the numerical simulation, the ground condition was simplified as moderately weathered sandstone. Its mechanical behavior was described using the Mohr-Coulomb (M-C) model, with soil parameters adopted from field data, as listed in Table 2. The geometric dimensions of the tunnel and support structures were based on the actual engineering values. The finite element model was discretized with 8-node linear brick, reduced integration elements (C3D8R), comprising a total of 93,756 elements and 104,583 nodes. The surrounding rock, pre-reinforced zone, initial support, and secondary lining were all simulated using solid elements, while the systematic rock bolts were modeled using line (truss) elements. As the advanced small pipes were installed within a 120 °arc at the tunnel crown in the field, the surrounding rock in this area was considered as an equivalent grouting layer in the model, with correspondingly increased ground parameters for the reinforced zone. The specific material parameters used in the model are detailed in Tables 2 and 3. The parameters for the surrounding rock and support structures were sourced from field data, while those parameters for the grouting layer were obtained through back-analysis based on the established model and monitored displacement data.

In the established model, the interactions between the initial support, secondary lining, and the soil were defined using tie constraints. The interactions between the rock bolts and both the initial support and the soil were simulated using the embedded region constraint. The tie constraint connects two separate surfaces, causing them to act as a single entity throughout the simulation without separation. Its primary advantage is that it eliminates the need to monitor the contact status of slave nodes or manage

their degrees of freedom during analysis, thereby significantly reducing computational time. The embedded region constraint, on the other hand, is used to embed a set of elements within another set of host elements, enforcing displacement compatibility between the embedded nodes and the host elements. Its key advantage lies in allowing the embedded elements (e.g., rock bolts) to be meshed independently and enabling the simulation of large-scale embedding of elements, such as rock bolts within the surrounding rock.

Table 2. Material parameters of surrounding rock and reinforcement zone by advanced small pipes.

Stratum type	Thickness, m	Density, kg/m^3	Elastic modulus, MPa	Poisson's ratio	Cohesion, kPa	Internal friction angle, °
Moderately weathered sandstone	230.0	2200	1470	0.35	190	25.6
Reinforced zone by advanced small pipes	4.5	2300	2000	0.30	250	32.0

Table 3. Material parameters of supporting structure.

Supporting structure	Density, kg/m^3	Elastic modulus, GPa	Poisson's ratio
Systematic rock bolts	7850	205.0	0.25
Initial support	2300	30.0	0.25
Secondary lining	2500	33.5	0.25

The tunnel excavation in the model followed the Core Soil Method with Annular Excavation, as illustrated in Figures 3 and 4. The sequence began with the excavation of the top annular crown section soil ①, during which the corresponding initial support and systematic rock bolts were installed simultaneously. Each analysis step in the model represented an excavation advance of 2 meters. After excavating the top annular section soil for two analysis steps (a total of 4 meters), the excavation of the upper core soil ② commenced.

Following the excavation of 4 meters of the upper core soil, the process moved to the excavation of the left-side lower bench soil ③. The installation of the initial support and systematic rock bolts for this corresponding section was carried out concurrently. To prevent the simultaneous unsupported exposure of both sides of a single steel rib, the excavation of the left and right sides of the lower bench soil was staggered by 3 to 5 meters. Consequently, after excavating 4 meters of the left-side lower bench soil, the excavation of the right-side lower bench soil ④ began, along with the installation of its corresponding initial support and systematic rock bolts.

Upon completing the excavation of 4 meters of the right-side lower bench soil, the installation of the secondary lining was initiated. The model subsequently repeated the entire sequence—excavating subsequent sections and installing the corresponding support structures—until the entire tunnel construction process was complete.

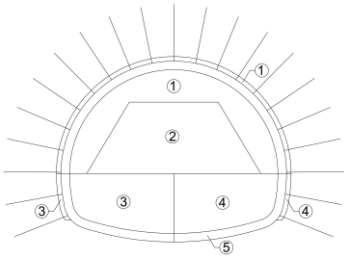

Figure 3. Schematic diagram of excavation sequence.

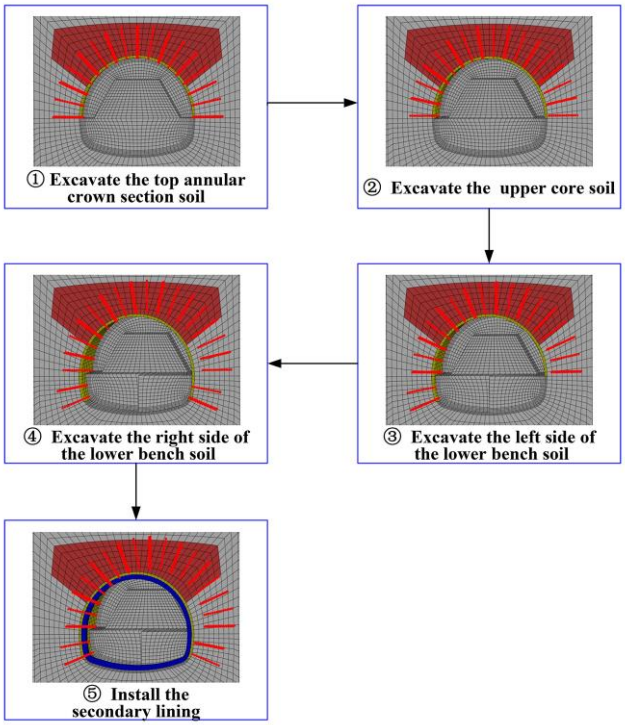

Figure 4. Excavation sequence of FEM model.

3.2. Model validation

Field monitoring was conducted at the construction site to measure the crown settlement of the surrounding rock and the horizontal convergence of the initial support. The layout of the monitoring points is shown in Figure 5. The crown settlement monitoring points were positioned at the tunnel vault, while the horizontal convergence measurement lines were located 1.5 meters above the spring line.

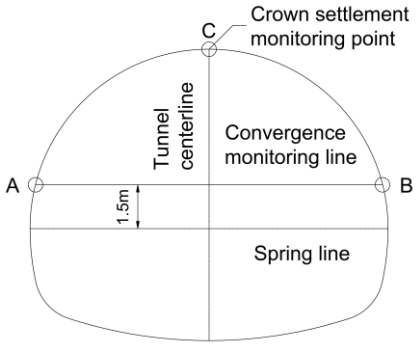

Figure 5. Schematic diagram of displacement monitoring points layout.

The numerical results for the crown settlement and initial support horizontal convergence at the central cross-section (y = 15 m) of the model under working condition 4—which employed the combined support scheme of advanced small pipes, initial support, systematic rock bolts, and a secondary lining—were extracted and compared with the field monitoring data, as shown in Figures 6 and 7. In the figures, negative values for crown settlement represent downward vertical displacement at the tunnel vault, and negative values for horizontal convergence indicate inward contraction of the tunnel towards its center.

Regarding the crown settlement of the surrounding rock, at analysis step 8—which corresponds to the excavation reaching the central cross-section—the value obtained from the numerical simulation is

−11.59 mm, while the field monitoring value is −12.57 mm, with a relative error of 7.79%. At analysis step 12, corresponding to the lower bench excavation reaching the central cross-section, the simulated settlement is −22.48 mm, and the monitored value is −23.41 mm, with a relative error of 3.97%. At analysis step 16, which involves the installation of the lining at the central cross-section, the simulated settlement result is −27.14 mm, compared to a field monitoring value of −26.58 mm, with a relative error of 2.11%. Finally, at analysis step 24, marking the completion of tunnel excavation and support, the numerical simulation yields a convergence value of −27.95 mm, while the field monitoring value is −27.9 mm, with a relative error of 0.18%.

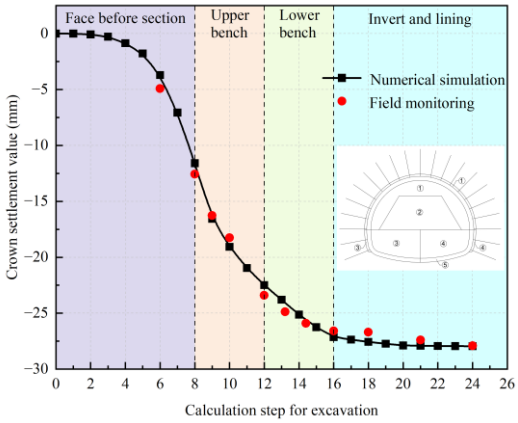

Figure 6. Comparison of crown settlement between numerical simulation and field measurement.

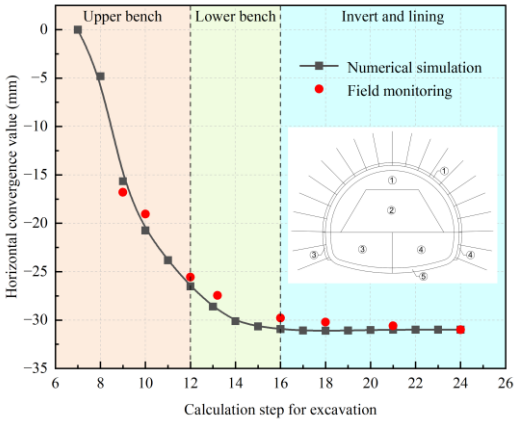

Figure 7. Comparison of horizontal convergence of initial support between numerical simulation and field measurement.

Regarding the horizontal convergence of the initial support, at analysis step 12—when the lower bench excavation reaches the central cross-section—the value obtained from the numerical simulation is −26.51 mm, while the field monitoring value is −25.56 mm, with a relative error of 3.72%. At analysis step 16, which involves the installation of the lining at the central cross-section, the simulated result is −30.92 mm, compared to a field monitoring value of −29.78 mm, with a relative error of 3.83%. Finally, at analysis step 24, marking the completion of tunnel excavation and support, the numerical simulation yields a convergence value of −30.99 mm, while the field monitoring value is −31 mm, with a relative error of 0.03%.

Comparison reveals that, except for the early stage of tunnel excavation when the crown settlement error reached 7.79% as the tunnel face just reached the monitoring cross-section, the errors for both settlement and convergence at all other key construction steps are within the range of approximately 2% to 3%, thereby validating the rationality of the finite element model.

4. Analysis of numerical simulation results

4.1. Analysis of surrounding rock vertical displacement

Table 4 presents the crown settlement values of the surrounding rock during key construction steps under the four working conditions, while Figure 8 illustrates the development pattern of crown settlement throughout the tunnel excavation process for all conditions. It can be observed that the settlement deformation trends are identical across the four working conditions, with the total deformation process divided into four distinct stages. The first stage spans from calculation step 1 (the start of excavation) to step 8, when the tunnel face reaches the monitoring cross-section. During this stage, the rate of crown settlement transitions from a slow initial increase to a more accelerated growth. The deformation of the surrounding rock under the four working conditions shows little discrepancy, remaining largely consistent.

The period from calculation step 8, when the tunnel face reaches the monitoring cross-section, to step 12, when the lower bench excavation reaches the monitoring cross-section, constitutes the second stage—the upper bench influence zone. During this stage, the annular crown section and the upper core soil are excavated, with the corresponding initial support and systematic rock bolts installed concurrently. Upon entering the upper bench influence zone, the crown settlement rate increases significantly, and the settlement values under the four working conditions begin to diverge. Condition 4 exhibits the smallest settlement, followed by Condition 3, then Condition 2, with Condition 1 showing the largest settlement. Throughout this stage, the advanced small pipes demonstrate a more pronounced effect on controlling crown settlement compared to the systematic rock bolts.

Table 4. Crown settlement values at key construction steps under different working conditions.

Working condition	Crown settlement value (mm)					
	Excavate the top annular crown section soil	Excavate the upper core soil	Excavate the left side of the lower bench soil	Excavate the right side of the lower bench soil	Install the secondary lining	Completion of excavation
Working condition 1	13.13	21.26	24.81	27.55	29.72	30.63
Working condition 2	12.85	20.67	23.91	26.45	28.43	29.20
Working condition 3	11.89	19.65	23.30	26.09	28.33	29.29
Working condition 4	11.59	19.06	22.48	25.13	27.14	27.95

Following the excavation of the upper annular crown section, the average crown settlement across the four working conditions is 12.37 mm, accounting for approximately 42.24% of the total settlement. Compared to the excavation of the upper annular crown section, the excavation of the upper core soil induces a marked increase in crown settlement, rising from an average of 12.37 mm to 20.16 mm—an increase of about 62.97%. This highlights the need for particular attention during this construction phase.

By the end of the upper core soil excavation, the crown settlement has reached 68.87% of the final settlement value.

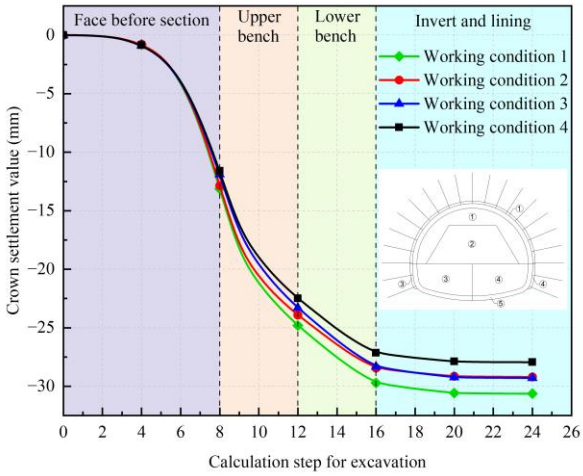

Figure 8. Development pattern of crown settlement under different working conditions during tunnel excavation.

The period from calculation step 12, when the lower bench excavation reaches the monitoring cross-section, to step 16, when the lining is installed at the monitoring cross-section, constitutes the third stage—the lower bench influence zone. The construction activities during this stage involve the sequential excavation of the left and right sides of the lower bench soil, along with the concurrent installation of the corresponding initial support and systematic rock bolts. Throughout this stage, the deformation rate of the surrounding rock begins to decrease, with crown settlement exhibiting a gradual and slow increase. The disparity in deformation between Working condition 1 and Working condition 4 widens compared to the second stage, whereas the difference between Working condition 2 and Working condition 3 narrows.

Following the excavation of the left side of the lower bench, the average crown settlement reaches 23.63 mm, accounting for approximately 80.71% of the total settlement. Subsequently, after the excavation of the left side of the lower bench, the crown settlement increases to 26.31 mm. This represents an increase of 2.68 mm, or about 11.34%, compared to the settlement after the left-side excavation. By the completion of the right-side lower bench excavation, the crown settlement has reached about 89.88% of the final settlement value.

The period from calculation step 16, when the lining is installed at the monitoring cross-section, to the final step 24, when tunnel excavation is completed, constitutes the fourth stage—the invert lining influence zone. During this stage, the deformation gradually stabilizes due to the installation of the secondary lining. The deformation disparity between Working condition 1 and Working condition 4 widens compared to the previous three stages, while the deformations in Working condition 2 and Working condition 3 remain largely consistent. Following the installation of the lining at the monitoring cross-section, the crown settlement value reaches 28.41 mm, accounting for approximately 97.05% of the total settlement.

Figure 9 illustrates the final magnitude and distribution of the vertical displacement in the surrounding rock under the four working conditions. It can be observed that the distribution characteristics of the vertical deformation are consistent across all conditions, manifesting as settlement

at the crown and heave at the invert. Figure 10, in turn, presents a comparative analysis of the maximum crown settlement values for the four working conditions. From Figure 9a and Figure 10, it is evident that for Working condition 1, which involves support provided solely by the initial support and secondary lining, the maximum crown settlement value is 34.23 mm, and the maximum invert heave value is 46.37 mm.

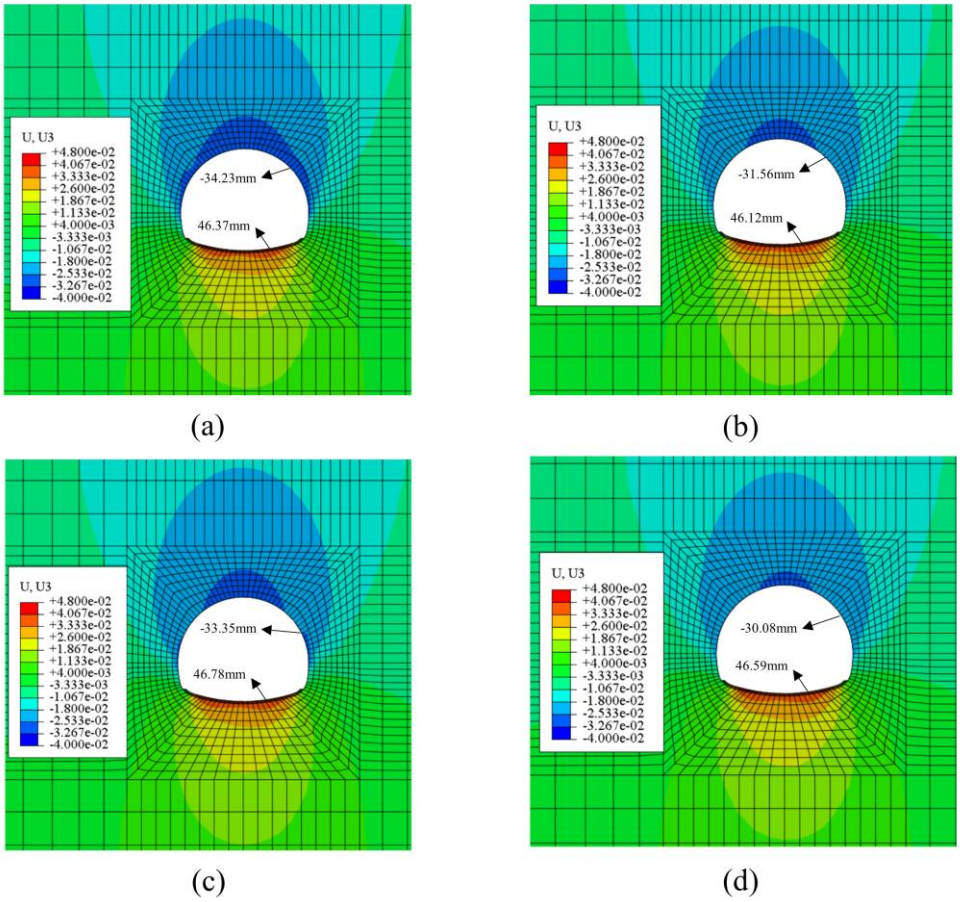

Figure 9. Contours of vertical displacement in surrounding rock under different working conditions. **(a)** Working condition 1; **(b)** Working condition 2; **(c)** Working condition 3; **(d)** Working condition 4.

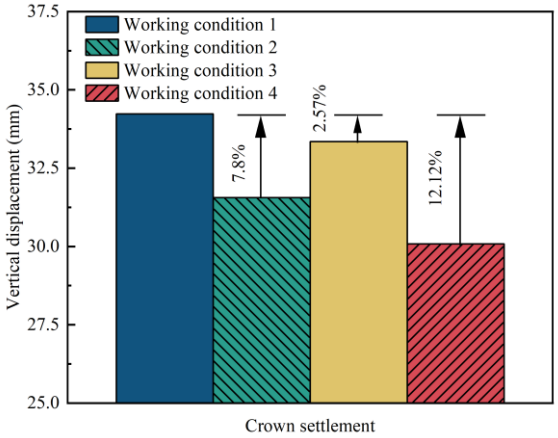

Figure 10. Comparison of maximum crown settlement in surrounding rock under different working conditions.

The application of systematic rock bolts and advanced small pipes leads to a measurable reduction in crown settlement across the corresponding working conditions. Under Working condition 2, which

incorporates rock bolt support, the maximum crown settlement decreases from 34.23 mm (Condition 1) to 31.56 mm, representing a reduction of approximately 7.80%. The maximum invert heave measures 46.12 mm, showing a slight decrease compared to condition 1.

In contrast, under Working condition 3, which employs advanced small pipes for support, the maximum crown settlement is reduced to 33.35 mm, a decrease of about 2.57%. However, the maximum invert heave shows a slight increase to 46.78 mm compared to Condition 1, although the magnitude of this change remains minimal. This variation is postulated to occur because the advanced small pipes are installed only within the crown region, providing limited reinforcement to the invert. Furthermore, their installation alters the internal stress distribution within the surrounding rock.

Under Working condition 4, which combines both support methods, the maximum crown settlement is 30.08 mm, representing a significant reduction of 12.12% compared to the base case (Condition 1). The maximum invert heave in this condition is 46.59 mm.

Therefore, the preceding analysis leads to the conclusion that the crown settlement process comprises four distinct stages, exhibiting a development pattern that transitions from a slow initial increase to a rapid acceleration, before finally stabilizing. The excavation of the upper core soil induces a period of significantly high settlement rate and magnitude, warranting particular attention during construction. Following the installation of the lining at the monitoring cross-section, the settlement rate essentially stabilizes. Regarding the specific settlement values, Condition 4 demonstrates the smallest final settlement, while Condition 1 shows the largest. During the early deformation stages, Condition 3 results in less settlement than Condition 2. However, after lining installation, Condition 2 exhibits lower settlement than Condition 3. As for the invert heave, Condition 2 shows the smallest value and Condition 3 the largest, although the overall variation is minimal, with a difference of less than 0.7 mm.

It can be observed that both systematic rock bolts and advanced small pipes contribute effectively to controlling crown settlement. The combined application of both methods in Condition 4 yields the best overall control effect. A comparison between Condition 2 and Condition 3 reveals that Condition 3 (advanced small pipes) provides superior settlement control in the initial construction phases, whereas Condition 2 (systematic rock bolts) demonstrates better control of the final settlement after the secondary lining is installed. This indicates that systematic rock bolts are more effective for long-term settlement control, while advanced small pipes serve as an effective pre-reinforcement measure.

4.2. Analysis of surrounding rock horizontal displacement

Figure 11 shows the horizontal displacement results of the surrounding rock under the four working conditions. It can be observed that the distribution characteristics of horizontal deformation are consistent across all conditions, all exhibiting a contraction pattern toward the tunnel center. The maximum displacement in each case is located at the arch springing. Figure 12 provides a comparative analysis of the magnitude of crown settlement under the four working conditions.

From Figure 11a and Figure 12, it can be seen that without the application of rock bolts and advanced small pipes, the maximum convergence displacement at the left arch springing of the tunnel is 43.33 mm, while the maximum convergence displacement at the right arch haunch is 39.71 mm. The horizontal displacement at the left arch springing is significantly greater than that at the right side. This is attributed to the fact that during tunnel excavation, the soil on the left side of the lower bench was excavated prior to the right side, resulting in the lower bench being in a non-uniform stress state during this phase.

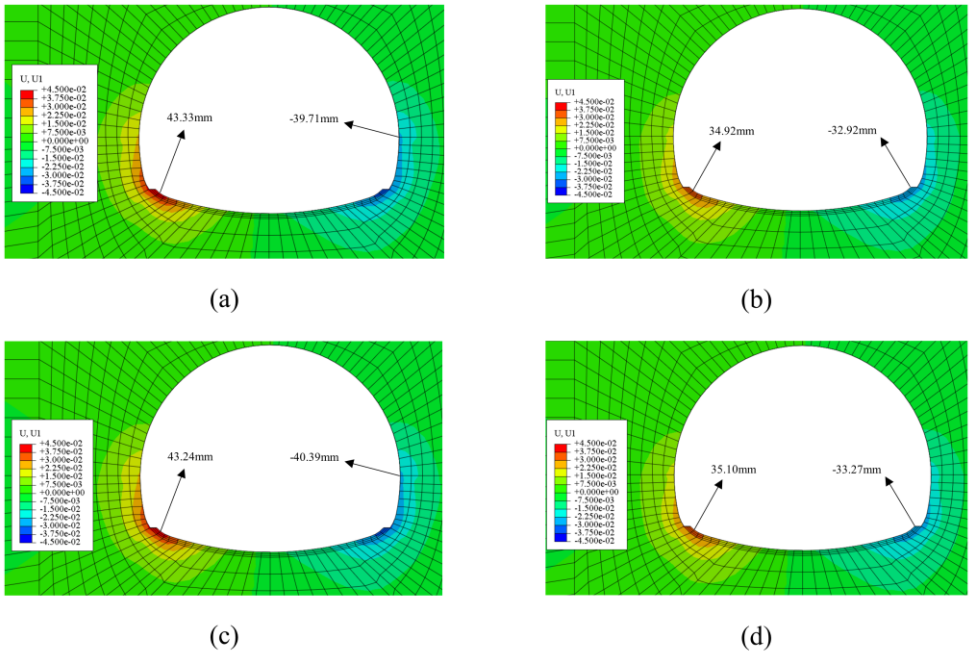

Figure 11. Contours of horizontal displacement in surrounding rock under different working conditions. **(a)** Working condition 1; **(b)** Working condition 2; **(c)** Working condition 3; **(d)** Working condition 4.

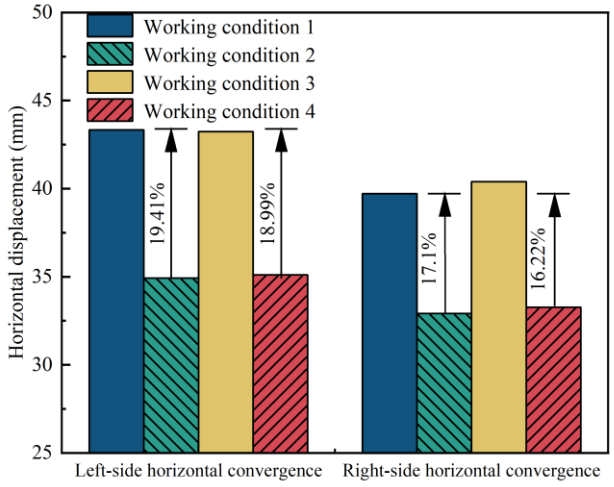

Figure 12. Comparison of maximum horizontal convergence in surrounding rock under different working conditions.

For Working condition 2, supported by systematic rock bolts, the maximum horizontal displacement at the left arch springing is 34.92 mm, representing a reduction of approximately 19.41% compared to Condition 1. The maximum horizontal displacement at the right arch springing is 32.92 mm, with a decrease of about 17.1%.

Under Working condition 3, which utilizes advanced small pipes for support, the maximum horizontal displacement at the left arch springing shows a slight decrease, with a convergence value of 43.24 mm. In contrast, the maximum horizontal displacement at the right arch springing experiences a minor increase, reaching a convergence value of 40.39 mm. However, the overall magnitude of this change remains minimal, representing an increase of only 1.71%.

In Working condition 4, where both support methods are combined, the maximum horizontal displacement at the left arch springing is 35.10 mm, reduced by 18.99%. The corresponding value at the right arch springing is 33.27 mm, showing a reduction of 16.22%.

In summary, regarding the horizontal convergence of the surrounding rock, Working condition 2 demonstrates the smallest value, followed by Working condition 4, then Working condition 1, with Working condition 3 exhibiting the largest convergence. Therefore, it can be concluded that systematic rock bolts are effective in controlling the horizontal displacement of the surrounding rock.

4.3. Analysis of initial support horizontal convergence

Table 5 presents the horizontal convergence values of the initial support during key construction steps of tunnel excavation under the four working conditions, while Figure 13 illustrates the development pattern of this convergence throughout the excavation process. The overall trend of convergence deformation is consistent across all four working conditions, and the total deformation process can be divided into three stages.

Table 5. Initial support horizontal convergence values at key construction steps under different working conditions.

Working condition	Horizontal convergence value (mm)					
	Excavate the top annular crown section soil	**Excavate the upper core soil**	**Excavate the left side of the lower bench soil**	**Excavate the right side of the lower bench soil**	**Install the secondary lining**	**Completion of excavation**
Working condition 1	4.67	23.13	31.07	36.09	37.23	37.29
Working condition 2	4.52	20.16	26.10	29.69	30.54	30.64
Working condition 3	5.10	23.86	31.54	36.39	37.49	37.52
Working condition 4	4.81	20.74	26.51	30.10	30.92	30.99

During the first stage, identified as the upper bench influence zone, the rate of horizontal convergence change is significant. The convergence values, which are initially nearly identical across all conditions, gradually separate into two distinct groups: the values for Working condition 2 and Working condition 4 are relatively close, with Condition 2 being slightly smaller than Condition 4; meanwhile, the values for Working condition 1 and Working condition 3 are also close, with Condition 1 being slightly smaller than Condition 3.

Following the excavation of the upper annular crown section and the installation of the corresponding initial support, the average horizontal convergence of the initial support across the four working conditions is 4.78 mm, accounting for approximately 14.1% of the final convergence deformation. Subsequently, after the excavation of the upper core soil, the horizontal convergence increases markedly from 4.78 mm to 21.97 mm, representing an increase of approximately 3.6 times. This indicates that the construction phase involving the excavation of the upper core soil requires particular attention.

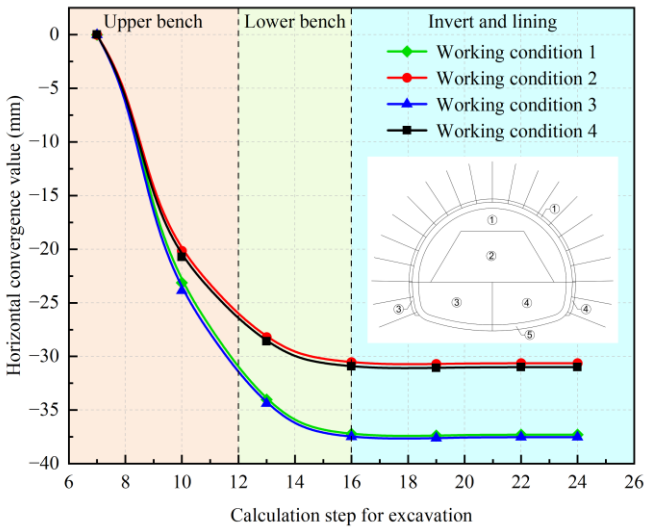

Figure 13. Development pattern of initial support horizontal convergence during tunnel excavation under different working conditions.

During the second stage, identified as the lower bench influence zone, the convergence rate of the initial support begins to decrease and essentially stabilizes by the end of this stage. Compared to the first stage, the disparity in horizontal convergence between the two previously identified groups—Working conditions 2 & 4 and Working conditions 1 & 3—further widens. Following the excavation of the lower bench's left side, the average horizontal convergence reaches 28.81 mm, accounting for approximately 84.53% of the final convergence deformation. Subsequently, after the excavation of the lower bench's right side, the horizontal convergence of the initial support further increases to 33.07 mm. This represents an increase of about 14.79% compared to the value recorded after the left-side excavation. Upon completion of the right-side lower bench excavation, the horizontal convergence of the initial support reaches 96.95% of its final value.

The third stage is identified as the invert lining influence zone. During this stage, the convergence deformation progressively stabilizes due to the installation of the secondary lining, with the deformation rate and magnitude both decreasing significantly. Following the lining installation, the average convergence of the initial support across the four working conditions is 34.05 mm, accounting for approximately 99.8% of the final convergence deformation.

It can be observed that the horizontal convergence deformation of the initial support under different working conditions primarily comprises three stages. Its development pattern is similar to that of crown settlement, transitioning from a slow initial increase to a rapid acceleration before finally stabilizing. The excavation of the upper core soil induces a period of significantly high convergence rate and magnitude, warranting particular attention during construction. Following the installation of the lining at the monitoring cross-section, the horizontal convergence essentially stabilizes. Working conditions 2 and 4 exhibit smaller horizontal convergence values, demonstrating that systematic rock bolts provide an effective control effect on the horizontal convergence of the initial support.

4.4. Analysis of surrounding rock stress field

Figure 14 illustrates the magnitude and distribution of the vertical stress in the surrounding rock under the four working conditions, while Figures 15–17 provide comparative analyses of the maximum tensile

stress, maximum compressive stress, and the compressive stress at the tunnel crown, respectively. As observed in Figure 14, tensile stress concentration occurs at the tunnel invert under all four working conditions, indicating that the tunnel is in a compressive failure mode.

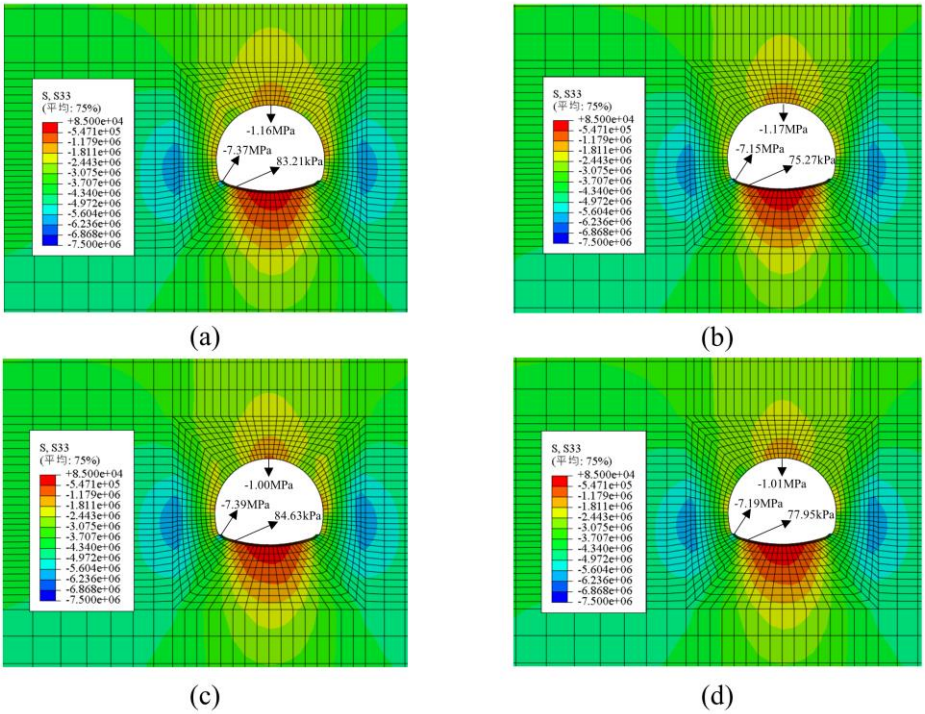

Figure 14. Contours of vertical stress in surrounding rock under different working conditions. **(a)** Working condition 1; **(b)** Working condition 2; **(c)** Working condition 3; **(d)** Working condition 4.

From Figures 14–17, it can be seen that in Working condition 1, the maximum tensile stress is 83.21 kPa, located slightly left of the tunnel invert; the maximum compressive stress is 7.37 MPa, situated at the left arch springing of the tunnel; and the vertical stress at the crown of the surrounding rock at the central cross-section (y = 15 m) is 1.16 MPa.

For Working condition 2, supported by systematic rock bolts, the maximum tensile stress in the surrounding rock decreases to 75.27 kPa, representing a reduction of approximately 9.54% compared to Condition 1. The maximum compressive stress is reduced to 7.15 MPa, which is 2.99% lower than in Condition 1. However, the vertical stress at the crown of the surrounding rock at the central cross-section (y = 15 m) shows a slight increase to 1.17 MPa.

Under Working condition 3, which utilizes advanced small pipes, the maximum tensile stress in the surrounding rock is 84.63 kPa, an increase of 1.71%. The maximum compressive stress reaches 7.39 MPa, showing a minor increase of 0.27%. In contrast, the vertical stress at the crown of the surrounding rock at the central cross-section (y = 15 m) is 1 MPa, representing a decrease of approximately 13.79%.

For Working condition 4, which combines both support methods, the maximum tensile stress in the surrounding rock is 77.95 kPa, reduced by 6.32%. The maximum compressive stress is 7.19 MPa, decreased by 2.44%. The vertical stress at the crown of the surrounding rock at the central cross-section (y = 15 m) is 1.01 MPa, lowered by approximately 12.93%.

Regarding the vertical stress in the surrounding rock, for both the maximum tensile stress and maximum compressive stress, Working condition 2 shows the smallest values, followed by Working

condition 4, then Working condition 1, with Working condition 3 exhibiting the largest values. Conversely, for the vertical stress at the tunnel crown, Working condition 3 demonstrates the smallest value, followed by Working condition 4, then Working condition 1, with Working condition 2 showing the largest value.

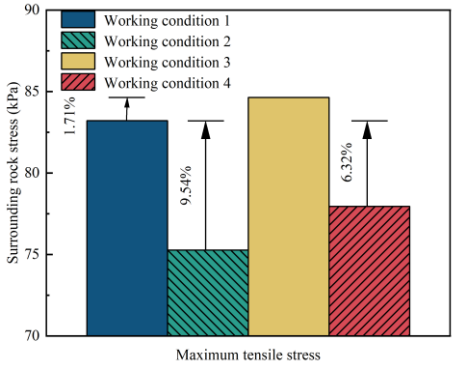

Figure 15. Comparison of maximum tensile stress in surrounding rock under different working conditions.

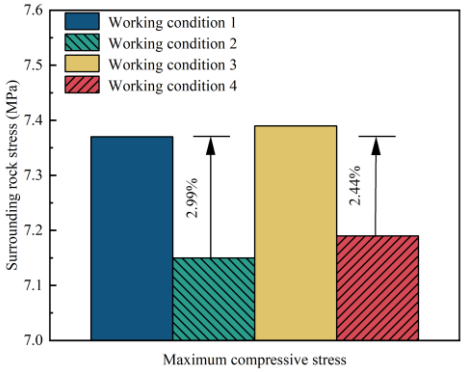

Figure 16. Comparison of maximum compressive stress in surrounding rock under different working conditions.

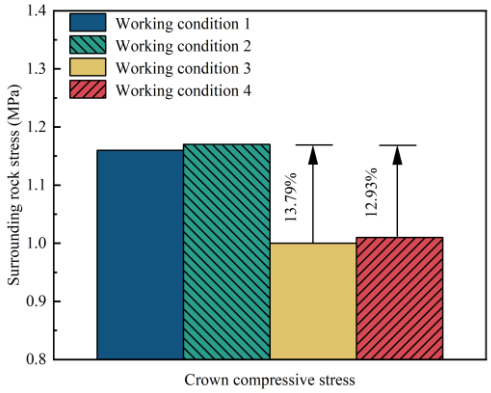

Figure 17. Comparison of crown compressive stress in surrounding rock under different working conditions.

4.5. Analysis of surrounding rock plastic zone

Figure 18 shows the distribution of the plastic zone in the surrounding rock under the four working conditions. It can be observed that the plastic zone is primarily distributed around the arch haunches and

arch springing. The application of systematic rock bolts and advanced small pipes suppresses the plastic zone to varying degrees, with Condition 4 showing the smallest plastic zone, followed by Condition 2, then Condition 3, and Condition 1 exhibiting the largest extent. This demonstrates that systematic rock bolts provide superior control over the plastic zone development compared to advanced small pipes.

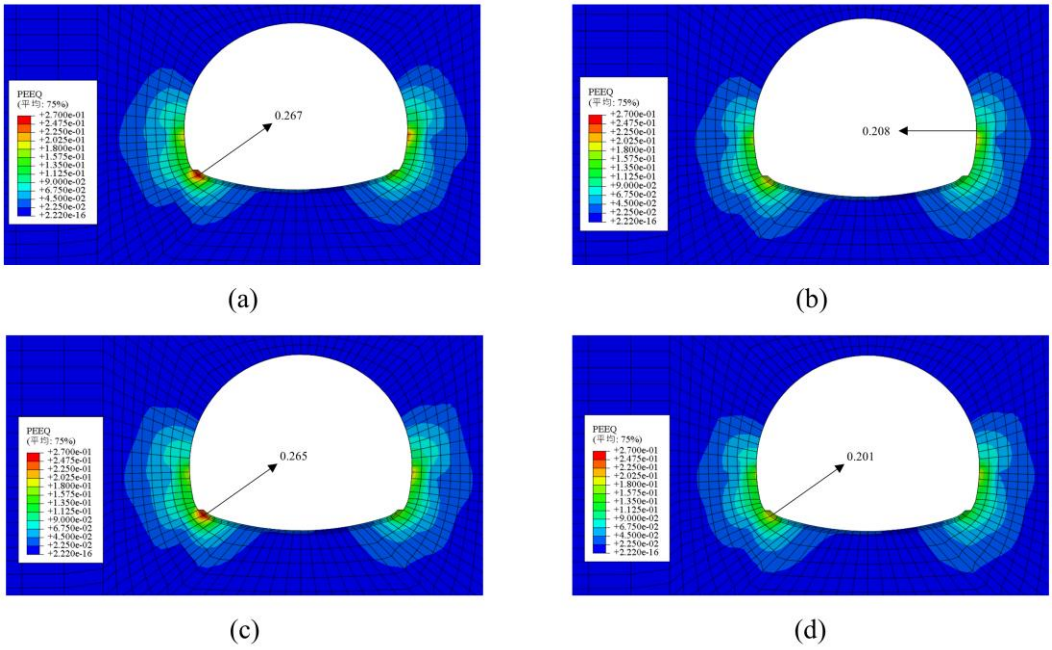

Figure 18. Contours of plastic zone in surrounding rock under different working conditions. **(a)** Working condition 1; **(b)** Working condition 2; **(c)** Working condition 3; **(d)** Working condition 4.

5. Analysis of construction cost

Based on the analysis of numerical simulation results presented above, Working condition 4 (*i.e.*, the combined support scheme) demonstrates the best performance in terms of controlling tunnel stress and deformation. Working condition 2, which utilizes systematic rock bolts, ranks second only to Condition 4 and even demonstrates an advantage in controlling horizontal convergence. In order to better compare the practical application effectiveness of Working condition 2 and Working condition 4 in real-world engineering and to further enhance the practical value of this study, this section conducts a further construction cost analysis focusing on the differential support measure between the two schemes—namely, the advanced small pipes. This analysis aims to provide a more comprehensive scheme comparison from another perspective.

As described in Section 2.2, the advanced small pipes in this study are installed within a 120 °arc at the tunnel crown, with a length of 4.5 m, a diameter of 42 mm, a circumferential spacing of 40 cm, and a longitudinal spacing of 320 cm. Based on relevant documentation provided by the project site and with reference to a similar engineering study, the construction cost of the advanced small pipes has been calculated [24]. The construction cost per meter of advance for the pipes is ¥17,033.6, meaning that Working condition 4 incurs this additional cost per meter compared to Working condition 2.

Integrating this with the conclusions from the simulation analysis, it can be observed that for deep-buried sections with relatively favorable surrounding rock conditions, the systematic rock bolt support scheme of Working condition 2 is sufficient to effectively control the stress and deformation of the surrounding rock while offering better project economy. For deep-buried sections with poorer surrounding rock

conditions, Working condition 4 can be adopted. In such cases, the advanced small pipes serve as an auxiliary construction method in weak and fractured zones, providing pre-reinforcement to the surrounding rock. Although this increases construction costs, it significantly enhances construction safety.

6. Conclusion

This study is based on the Xinjin Expressway spiral tunnel group, taking the Hankou Tunnel—a typical deep-buried section in weak and fractured strata—as the research object. Using the ABAQUS numerical simulation platform, a detailed numerical model of the full construction sequence was developed. Based on the composite lining structure of initial and secondary support, four working conditions considering the presence and absence of systematic rock bolts and advanced small pipes were established in the numerical model, which was subsequently validated against field monitoring data. By comparing the simulation results, the stress and deformation behavior of the surrounding rock under different working conditions and at various construction stages was analyzed, leading to a comparative evaluation of multiple support schemes. The following conclusions are drawn:

(1) Under all four working conditions, both the crown settlement and horizontal convergence exhibit a consistent development pattern during tunnel excavation: an initial phase of slow growth, followed by a period of rapid increase, before eventually stabilizing. The rate and magnitude of change in crown settlement and horizontal convergence increase significantly during the excavation of the upper core soil, which occurs after the installation of the initial support. However, following the application of the secondary lining, the rate of change for both parameters essentially stabilizes.

(2) The application of systematic rock bolts can effectively control the crown settlement, horizontal convergence, and plastic zone development of the surrounding rock. In contrast, the use of advanced small pipes demonstrates a more notable effect in controlling crown settlement and the stress state at the crown.

(3) Regarding the control of vertical stress at the tunnel crown, advanced small pipes prove more effective than systematic rock bolts. However, systematic rock bolts exhibit superior performance in controlling horizontal convergence, maximum tensile stress, and the extent of the plastic zone.

(4) Taking into account both numerical simulation results and the construction cost analysis, the combined support scheme consisting of primary support, secondary lining, and systematic rock bolts represents a more suitable choice for deep-buried sections with relatively favorable surrounding rock conditions. Whereas, advanced small pipes can be adopted as an auxiliary construction method in weak and fractured zones, providing essential pre-reinforcement to the surrounding rock.

7. Limitations and future work

This study explored support strategies for deep-buried soft and broken tunnel sections. The limitations and future research directions are outlined below:

(1) To enhance computational efficiency, the advanced small pipes in this study were equivalently modeled as a grouting layer with parameters determined through back-analysis. Future research could consider modeling the pipes as solid elements to achieve a more detailed and refined representation, thereby enabling a more realistic simulation of their reinforcement effect and a deeper investigation into their efficacy.

(2) This simulation study employed support parameters from actual engineering practice to investigate and compare the reinforcement effectiveness under four different working conditions. However, the influence of varying support parameters on the overall support effect was not explored. Future research could incorporate parametric analyses to comparatively study the impact of different support parameters on tunnel structural support performance, and subsequently evaluate or optimize the engineering parameters adopted for on-site construction.

(3) This study focused on analyzing deformation patterns exclusively at the longitudinal central cross-section of the tunnel. Consequently, the longitudinal length of the tunnel model was set to only 30 meters, and the influence of curvature was not considered. Future studies could extend the longitudinal dimension of the tunnel model to investigate deformation patterns along the tunnel axis. Additionally, incorporating curvature into the modeling process to explore its effects would be a valuable direction for further research.

Data availability statement

No supplementary or additional data were generated in this study. All data generated during this study were included in this published article.

Acknowledgments

This work was funded by National Natural Science Foundation of China with grant number 52278385.

Authors' contribution

Dechun Lu: conceptualization, methodology, investigation, data curation, formal analysis, writing—original draft, visualization. Xiaoyu Liu: methodology, software, data curation, validation, writing—original draft, visualization. Haining Xu: data curation, funding acquisition, resources, supervision, project administration, writing—review & editing. Caixia Guo: conceptualization, methodology, supervision, project administration, writing—review & editing. Xiuli Du: conceptualization, supervision, resources, project administration, writing—review & editing. All authors have read and agreed to the published version of the manuscript.

Conflicts of interest

Xiuli Du holds the position of Editor-in-chief for *Smart Construction* and has not peer reviewed or made any editorial decisions for this paper.

References

[1] Lee CJ, Chiang KH, Kuo CM. Ground movement and tunnel stability when tunneling in sandy ground. *J. Chin. Inst. Eng.* 2011, 27(7):1021–1032.

[2] Lei M. Study on supporting structure of highway tunnel with soft surrounding rock (In Chinese). Master's Thesis, Southwest Jiaotong University, 2012.

[3] Yang Z, Gao Y, Wu S, Cheng Z. Optimization study of first liner replacement timing of large deformation tunnel based on convergence-constraint principle (In Chinese). *Rock Soil Mech.* 2018, 39(S1):395–404.
[4] Qin S. Research on deformation and bearing capacity of flexible support in weak rock masses tunnel (In Chinese). Master's Thesis, Xi'an University of Architecture and Technology, 2019.
[5] Wang J, Lin G. Study on the characteristics of secondary lining cracking under the effect of rheological load (In Chinese). *Mod. Tunnelling Tech.* 2020, 57(1):83–90.
[6] Chen L, Chen J, Luo Y, Liu W, Wang C. Deformation law and reasonable reserved deformation of deep large-span chlorite schist tunnel (In Chinese). *China J. Highw. Transp.* 2021, 34(06):147–157.
[7] Tian S, Wang W, Gong J. Development and prospect of railway tunnels in China (including statistics of railway tunnelsin China by the end of 2020) (In Chinese). *Tunnelling Constr.* 2021, 41(2):308–325.
[8] Qing W, Zhu Y, Zhang H. Research on mechanical characteristics of anchor bolts of shallow-buried four-track railway station tunnel (In Chinese). *Tunnelling Constr.* 2021, 41(5):749–757.
[9] Zhou J. Study on the bearing mechanism of composite lining in deep-buried mountain tunnels (In Chinese). Doctoral Thesis, Tongji University, 2022.
[10] Bobet A, Einstein HH. Tunnel reinforcement with rockbolts. *Tunnelling Underground Space Technol.* 2011, 26(1):100–123.
[11] Chen S, Zhang Q. Test analysis of anchoring effect of weak interlayer in Xianglushan Tunnel (In Chinese). *Water Resour. Power* 2019, 37(9):104–107.
[12] Tian Z, Lin G, Yang F, Jiang Y, Wang B. Experimental test of support effect of different tunnel support systems (In Chinese). *Mod. Tunnelling Tech.* 2018, 55(2):134–139.
[13] Tan Z, Yu Y, Wang M, Yang J. Experimental research on bolt anchorage effect on large-section deep-buried tunnel in loess (In Chinese). *Chin. J. Rock Mech. Eng.* 2008, (8):1618–1625.
[14] Shi Z, Li X, Chen B. A test study of the effect of systematic bolts for the Lijiazhai tunnel in Guizhou (In Chinese). *Hydrogeol. Eng. Geol.* 2020, 47(1):80–88.
[15] Sun X, Li X, Wang W. Experimental study of support effect of system bolts of a deeply-buried large-span tunnel in moderately-weathered mudstone (In Chinese). *Tunn. Constr.* 2023, 43(S2):151–161.
[16] Jin C, Xia Z, Xiang C, Dong L, Zhao P, *et al.* Numerical simulation of advanced small pipe in tunnels during excavation by steps. *Appl. Mech. Mater.* 2013, 2545(353–356):3699–3702.
[17] Qin C, Huang M, Pan M. Numerical analysis of grouting with advanced micropipe support effect in the large section and weak surrounding rock tunnel (In Chinese). *Technol. Econ. Areas Commun.* 2018, 20(3):76–80.
[18] Liu K, Li S, Ding W, Hou M, Gong Y, *et al.* Pre-supporting mechanism and supporting scheme design for advanced small pipes in the silty clay layer. *Tunn. Undergr. Sp. Tech.* 2020, 98:103259–103259.
[19] An Y, Zhou J, Ouyang P, Li J. Analysis of tunnel face stability with advanced pipes support. *J. Cent. South Univ.* 2021, 28(2):604–617.
[20] Wang Y, Liu J. Deformation analysis of small spacing tunnels in soft rock under different advance support consitions (In Chinese). *J. Inner Mong. Univ. Sci. Tech.* 2024, 43(4):342–347.

[21] Zhang H, Wang Z, Wan F, Li Y, Liao W, *et al.* Effectiveness of advanced support for shallow-buried tunnel excavation under-crossing provincial highway in water-rich fractured zone (In Chinese). *Pearl River* 2025, 46(11):35–43.

[22] Li Z, Chen R, Meng F, Ye J. Tunnel boring machine tunneling-induced ground settlements in soft clay and influence of excavation parameters (In Chinese). *J. Zhejiang Univ.* 2015, 49(7):1268–1275.

[23] Vitali OPM, Celestino TB, Bobet A. Buoyancy effect on shallow tunnels. *Int. J. Rock Mech. Min.* 2019, 114:1–6.

[24] Chen G, Wang Z, Chen J, Yan Q, Gong F, *et al.* Comprehensive evaluation of overrun support optimization for sanded dolomite tunnels based on combinatorial assignment (In Chinese). *Chin. Rural Water Hydropower* 2024, (11):233–239,246.